DOI: 10.1002/ejic.200700382

New Single-Molecule Magnets by Site-Specific Substitution: Incorporation of "Alligator Clips" into Fe_4 Complexes

Anne-Laure Barra,[a] Federica Bianchi,[b] Andrea Caneschi,[c] Andrea Cornia,*[d] Dante Gatteschi,[c] Lapo Gorini,[c] Luisa Gregoli,[d] Monica Maffini,[b] Francesca Parenti,[d] Roberta Sessoli,*[c] Lorenzo Sorace,[c] and Anna Maria Talarico[d]

Keywords: Iron / Ligand design / Magnetic properties / EPR spectroscopy / Single molecule magnets

"Alligator clips" suitable for grafting on H-terminated silicon or gold surfaces have been incorporated into single-molecule magnets (SMMs) of the Fe_4 family. Tripodal ligands 2,2-bis-(hydroxymethyl)-10-undecen-1-ol (H_3L^1) and 11-(acetylthio)-2,2-bis(hydroxymethyl)undecan-1-ol (H_3L^2) have been used to replace the six methoxide bridges in $[Fe_4(OMe)_6(dpm)_6]$, affording new Fe_4 derivatives $[Fe_4(L^1)_2(dpm)_6]$ (**1**) and $[Fe_4(L^2)_2(dpm)_6]$ (**2**) in high yield (Hdpm = dipivaloylmethane). The molecular structures have been unambiguously established by XRD combined with ESI-MS and magnetic characterization techniques, including DC and AC magnetometry and high-frequency EPR spectroscopy. The two SMMs have an $S = 5$ ground state and an easy-axis magnetic anisotropy leading to slow relaxation of the magnetization at low temperature, with effective anisotropy barriers of 15.9(2) K in **1** and 15.1(2) K in **2**.

Introduction

Single-molecule magnets (SMMs) are among the smallest magnetic structures that can be conceived, consisting of only a few magnetic atoms. The constituent magnetic units are d-block transition-metal or, more rarely, rare-earth ions.[1–3] The unique feature of SMMs is their large-spin ground state associated with a substantial easy-axis magnetic anisotropy. As a result, the "giant" total magnetic moment experiences a molecular anisotropy barrier U_{eff}, which governs relaxation. At sufficiently low temperatures the relaxation of the magnetic moment becomes so slow that hysteresis appears when the external field is cycled. In this respect, spin reversal occurs through a classical, thermally activated mechanism and is very similar to that observed in magnetic nanoparticles. However, because of the discreteness of the spin levels in SMMs, magnetic moment reversal may also occur through quantum tunneling (QT), giving rise to stepped hysteresis loops and making SMMs unique magnetic systems.[2]

In the last decade, SMM research has mainly focussed on large molecular assemblies such as single crystals, polycrystalline samples, solutions, and Langmuir–Blodgett films. The advances in nanotechnology nowadays enable the study of molecular magnetism in lower-dimensional systems.[4] For example, with scanning probe microscopy (sub)-monolayers of SMMs at surfaces are studied extensively.[5] Moreover, researchers have now reached the ultimate limit of electronic devices by connecting two wires to a single molecule, measuring the flow of electrons through it, and controlling this flow with a nearby gate electrode.[6] In this context, a key step is the development of strategies to introduce specific functionalities, like surface-binding sites, around the core of SMMs, without altering the magnetic behavior. As the grafting protocols usually involve liquid-phase operations, the complexes should additionally remain intact in solution and on surfaces. We are currently pursuing the functionalization of SMMs in order to realize molecular wires containing high-spin units that may be grafted on surfaces or linked to proximal electrodes. In a previous paper we demonstrated that four surface-binding groups can be linked to the core of Mn_{12}-type SMMs using proper ligand design.[7]

In this paper, we report the successful preparation of two novel iron(III)-based SMMs that exhibit a wire-like molecular geometry, **1** and **2** (Figure 1). The complexes feature long-chain alkyl tethers at opposite sides and terminal "alligator clips" of two different types: alkenyl (**1**) and thioacetyl (**2**) groups, which can be used for deposition on H-ter-

[a] Grenoble High Magnetic Field Laboratory – CNRS, 25 Avenue des Martyrs, 38042 Grenoble Cedex 9, France
[b] Department of General and Inorganic Chemistry, Analytical Chemistry, Physical Chemistry, Università degli Studi di Parma, Viale G. P. Usberti 17/A, 43100 Parma, Italy
[c] La. M. M., Department of Chemistry and INSTM Research Unit, Università degli Studi di Firenze, Via della Lastruccia 3, 50019 Sesto Fiorentino (FI), Italy
Fax: +39-55-4573372
E-mail: roberta.sessoli@unifi.it
[d] Department of Chemistry and INSTM Research Unit, Università degli Studi di Modena e Reggio Emilia, Via G. Campi 183, 41100 Modena, Italy
Fax: +39-59-373543
E-mail: acornia@unimore.it
Supporting information for this article is available on the WWW under http://www.eurjic.org or from the author.

minated silicon[8a] and gold[8b] substrates, respectively. Using DC and AC magnetometry and HF-EPR spectroscopy, we additionally show that the site-specific functionalization occurs with full retention of the magnetic properties.

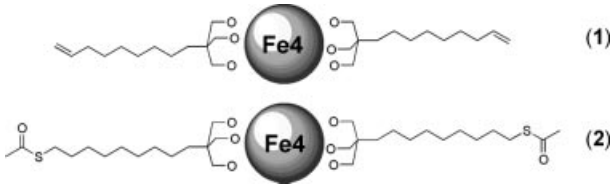

Figure 1. Approach to Fe_4-based SMMs with a wire-like geometry.

Results and Discussion

Synthesis

The derivatives of 2-(hydroxymethyl)propane-1,3-diol, $RC(CH_2OH)_3$, are widely used as versatile ligands in transition-metal chemistry because they can adopt a large variety of binding modes.[9] The $\eta^2,\eta^2,\eta^2,\mu_4$ mode is found in simple metal-centered Fe^{III} triangles, commonly known as "ferric stars", which have an $S = 5$ ground state and behave as SMMs with energy barriers as high as 17 K.[10] The synthesis is very conveniently carried out starting from the archetypal Fe_4 compound $[Fe_4(OMe)_6(dpm)_6]$ (**3**) (Hdpm = dipivaloylmethane).[11] At variance with other "ferric stars",[5b,12] the bridging methoxide groups in **3** can be easily exchanged, leaving the bulky shell of terminal dpm^- anions unchanged. The binding geometry of the tripods is such that the R groups lie on opposite sides of the flat Fe_4 moiety, thus providing access to molecular wire-like geometries (Figure 1).

In order to attach surface-binding functionalities to the Fe_4 core, we used the tripods 2,2-bis(hydroxymethyl)-10-undecen-1-ol (H_3L^1) and 11-(acetylthio)-2,2-bis(hydroxymethyl)undecan-1-ol (H_3L^2). The former was prepared from 10-undecenal and excess formaldehyde[13a] by Tollens condensation. The terminal double bond of H_3L^1 undergoes addition of thioacetic acid in the presence of 2,2′-azobis(2-methylpropionitrile) (AIBN) to afford the thioacetyl derivative H_3L^2 in moderate yield (Scheme 1).[13b]

The coordinating ability of the tripods H_3L^1 and H_3L^2 was first tested using ^2H NMR spectroscopy. Solutions of $[Fe_4(OMe)_6([D_{18}]dpm)_6]$ (**3D**) in dry Et_2O are known[10a] to exhibit time-dependent spectra, which reveal progressive decomposition to afford monomeric Fe(dpm) species. By contrast, after the addition of excess tripodal ligands (R = Ph or Me), the spectra show persistent peaks at $\delta = 10.3$ and 12.7 ppm, arising from polynuclear iron(III) complexes (Fe_4 or structurally related species) and magnetically uncoupled Fe(dpm) complexes, respectively. From the same solutions, doubly substituted Fe_4 derivatives can be isolated in high yield.[10a,10b] Similar results were obtained with the two tripodal ligands prepared in this work. The spectra recorded several hours after the addition of H_3L^1 or H_3L^2 (2.7 equiv.) to a solution of **3D** in dry Et_2O are characterized by peaks at $\delta = 10.3$ and 12.7 ppm in a 3:1 ratio (Figure 2a), suggesting that the coordinating ability of both H_3L^1 and H_3L^2 is comparable with that of simpler triols. The Fe_4 derivatives **1** and **2** could indeed be isolated in crystalline form (90–95% yield) by mixing **3** with an excess of

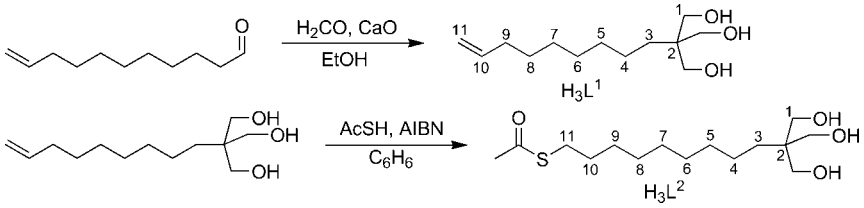

Scheme 1.

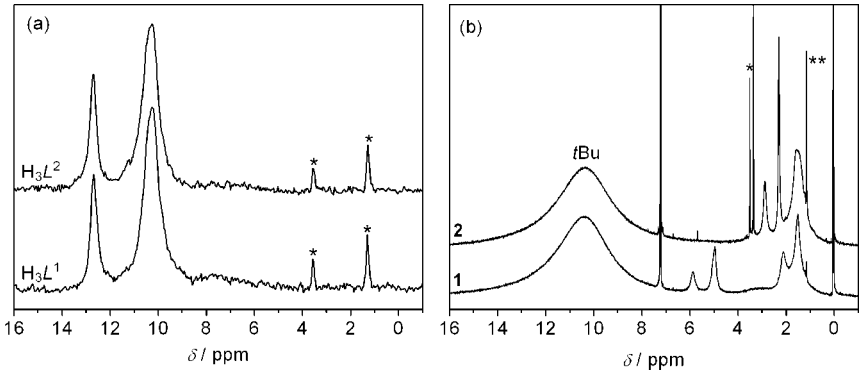

Figure 2. (a) ^2H NMR spectra of an Et_2O solution of **3D** recorded 18 h after the addition of H_3L^1 or H_3L^2 (2.7 equiv.). The signals labeled with * are due to the solvent. (b) ^1H NMR spectra of **1** and **2** in $CDCl_3$. The sharp signals indicated with * and ** are due to traces of dimethoxyethane and free Hdpm, respectively.

the appropriate tripodal ligand in an organic solvent and by either slow diffusion of methanol vapors or slow concentration.

Characterization

In spite of the presence of the long C_9 chains, compound $[Fe_4(L^1)_2(dpm)_6]$ (**1**) crystallizes in large X-ray-quality blocks that were investigated by X-ray diffraction methods at 120 K. The crystals belong to monoclinic space group *C*2/*c* and the lattice contains no crystallization solvent. The molecular structure has crystallographic C_2 symmetry, which has a twofold axis passing through Fe atoms Fe1 and Fe2 (Figures 3 and 4), but closely approaches D_3 symmetry. Selected interatomic distances and angles are gathered in Table 1.

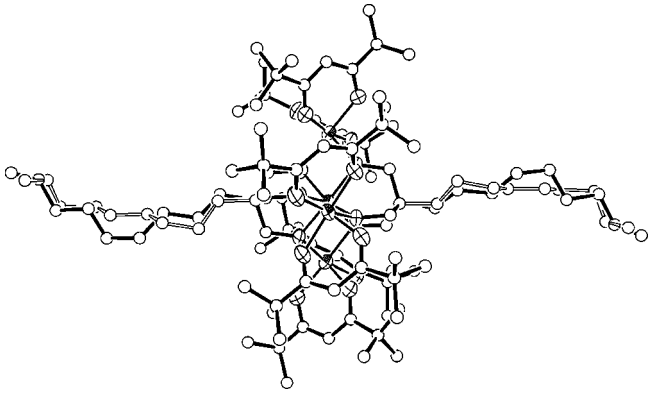

Figure 3. Molecular structure of **1** viewed approximately along the twofold axis. Iron and oxygen atoms are represented as 75%-probability ellipsoids, while carbon atoms are represented as spheres. H atoms have been omitted for clarity. The two positions occupied by the C_9 chain are drawn using solid and open bonds.

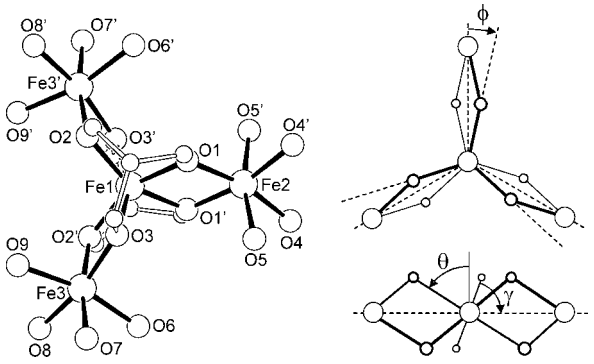

Figure 4. Left: structure of the Fe/O core in **1**, with four carbon atoms of the tripodal ligands and the atom-labeling scheme. Right: definition of the angles ϕ, θ, and γ. The dashed lines lie in the plane defined by the four metal centers.

The propeller-like structure of the precursor is retained, but replacement of the methoxide bridges with tripodal ligands leads to significant alterations of the core geometry (Figure 4). Assuming idealized D_3 symmetry, the angles θ and ϕ, which define trigonal compression/elongation and trigonal rotation for Fe1, are 54.2° and 30.8°.[14] While θ differs from the octahedral value (54.74°) by less than 1°, ϕ departs from the value found in regular octahedral symmetry (60°) by almost 30°. Therefore, the dominant type of distortion for Fe1 is trigonal rotation, which is directly related to the propeller's pitch γ (69.7°).[10a] Within the series of Fe_4 propellers so far synthesized, the structure of the Fe/O core in **1** is found to be intermediate between those observed for R = Me (θ = 54.1°, ϕ = 29.2°, γ = 70.8°) and Ph (θ = 54.2°, ϕ = 32.3°, γ = 68.8°), while it is very different from that of the precursor **3** (θ = 57.3°, ϕ = 37.7°, γ = 63.2°).[10a,10b] As shown in Figure 3, the C_9 chains of the tripodal ligands are directed along the idealized threefold molecular axis and are disordered on two equally populated positions. The molecular size, evaluated from the distance between the two C11 carbon atoms (Scheme 1), is 2.5–2.6 nm.

Table 1. Selected interatomic distances [Å] and angles [°] for **1**.[a]

Fe1···Fe2	3.0808(8)	Fe1···Fe3	3.0919(4)
Fe2···Fe3	5.2304(6)	Fe3···Fe3′	5.5652(6)
Fe1–O2	1.9774(17)	Fe1–O1′	1.9846(18)
Fe1–O3	1.9924(15)	Fe2–O1	1.9728(19)
Fe2–O5	1.9923(16)	Fe2–O4	2.0038(19)
Fe3–O3	1.9578(16)	Fe3–O7	1.9905(16)
Fe3–O2′	1.9944(16)	Fe3–O8	1.9972(17)
Fe3–O9	2.016(2)	Fe3–O6	2.0284(18)
Fe2···Fe1···Fe3	115.85(1)	Fe3···Fe1···Fe3′	128.30(2)
Fe3···Fe2···Fe3′	64.28(1)	Fe2···Fe3···Fe3′	57.86(1)
O1′–Fe1–O1	77.48(10)	O2–Fe1–O1′	155.54(7)
O2–Fe1–O1	88.67(7)	O2–Fe1–O2′	110.69(11)
O1′–Fe1–O3	108.75(7)	O1–Fe1–O3	88.40(7)
O2–Fe1–O3	90.66(7)	O2′–Fe1–O3	76.96(6)
O3–Fe1–O3′	158.31(11)	O1–Fe2–O1′	78.03(10)
O1–Fe2–O4	167.41(8)	O1′–Fe2–O4	92.01(7)
O4–Fe2–O4′	98.81(12)	O5–Fe2–O4	85.60(7)
O5′–Fe2–O4	85.92(7)	O1–Fe2–O5	88.81(8)
O1′–Fe2–O5	101.38(7)	O5–Fe2–O5′	166.95(13)
O3–Fe3–O2′	77.36(6)	O7–Fe3–O2′	170.01(8)
O3–Fe3–O6	102.04(8)	O7–Fe3–O6	85.22(7)
O2′–Fe3–O6	89.25(7)	O8–Fe3–O6	84.92(7)
O9–Fe3–O6	166.91(7)	O3–Fe3–O7	95.64(7)
O3–Fe3–O8	166.36(7)	O7–Fe3–O8	96.63(7)
O2′–Fe3–O8	91.15(7)	O3–Fe3–O9	89.09(7)
O7–Fe3–O9	86.86(7)	O2′–Fe3–O9	100.02(8)
O8–Fe3–O9	85.66(8)	Fe2–O1–Fe1	102.24(7)
Fe1–O2–Fe3′	102.24(7)	Fe1–O3–Fe3	103.02(7)

[a] Symmetry transformations used to generate equivalent atoms: ′: $-x + 1$, y, $-z + 3/2$.

The second compound, $[Fe_4(L^2)_2(dpm)_6]$ (**2**), was isolated as weakly diffracting orange crystals, which turned out to be unsuitable for X-ray analysis. Structure elucidation was then based on elemental analysis, spectroscopic and spectrometric (ESI-MS) methods. The ^1H NMR spectra of **1** and **2** in $CDCl_3$ are compared in Figure 2b. In **1**, the very broad signal of paramagnetically shifted *t*Bu protons at δ = 10.4 ppm is accompanied by additional resonances at δ = 5.91 (2 H), 5.00 (4 H), and 2.16 (4 H) ppm due to C10, C11, and C9 hydrogen atoms, respectively, which undergo small paramagnetic shifts.[13a]

However, the signal from the CH_2O hydrogen atoms of the tripod, which is observed as a sharp singlet at δ = 3.75 ppm in H_3L^1,[13a] is completely absent in the spectrum,

as expected because of the proximity of CH_2O hydrogen atoms to the paramagnetic metal centers. Similarly, the broad peak at $\delta \approx 1.5$ ppm integrates to about 16 H per molecule, and does not account for the remaining 24 aliphatic protons. The four CH_2 groups closer to the metal core are presumably paramagnetically shifted and broadened beyond detection, as suggested by the very broad signal observed at $\delta \approx 3$ ppm. Therefore, spectroscopic data strongly indicate that the solid-state structure of **1** is fully retained in solution. The ^1H NMR spectrum of **2** in $CDCl_3$ shows, in addition to the broad *t*Bu signal, two resonances at $\delta = 2.89$ (4 H) and 2.31 (6 H) ppm due to C11 and acetyl hydrogen atoms, respectively, and no signal from CH_2O protons. Again, the broad peak at $\delta \approx 1.5$ ppm integrates to about 24 H, as expected assuming that two CH_2 groups per tripodal ligand are not detectable. The UV/Vis absorption spectra of **1** and **2** in toluene solution are identical (Figure S1). They have two bands at 349 and 400 nm assigned to $t_{2g} \rightarrow \pi^*$ and $\pi \rightarrow t_{2g}$ charge transfer transitions, respectively, involving the β-diketonate ligands.[15] The solid-state IR spectra denote a strong similarity between the two structures, except for the presence of the characteristic absorptions due to the different terminal functionalities (Figure S2). In particular, in **1** the absorption bands typical of alkene groups are observed at 909, 994, and 1644 cm^{-1}, corresponding to –C=C–H in-plane and out-of-plane bending and C=C stretching modes, respectively. In **2** these bands are not present, but we find a new strong absorption at 1699 cm^{-1} typical of the stretching vibration of the acetyl C=O group. We conclude that, according to ^1H NMR, UV/Vis, and IR spectroscopy, the structures of **1** and **2** in the solid state and in solution are strictly similar.

Electrospray ionization mass spectrometry (ESI-MS) was additionally used for the characterization of **1** and **2**. Owing to the capability of providing an accurate determination of the molecular mass of relatively large and labile molecules,[16] this soft ionization technique has been widely used for the characterization of cationic complexes as well as in the study of metal-ion-induced self-assembly processes and SMMs.[17] In this study, **1** and **2** were dissolved in dichloromethane/nitromethane (2:1) and directly infused into the electrospray mass spectrometer system. The experimental isotope clusters obtained are in agreement with the theoretical masses and reconstructed ESI isotope patterns, thus increasing the confidence in the identification.

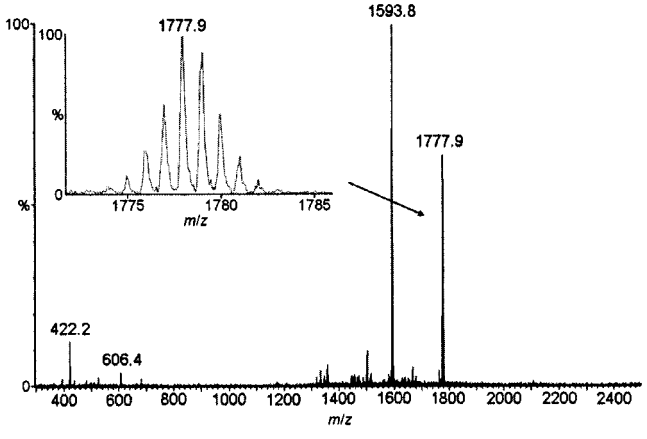

Figure 5. ESI(+)-MS full scan spectra of **1**. The inset shows a mass-scale-expanded segment of the ion signal at $m/z = 1777.9$ attributable to the $[\mathbf{1} + H]^+$ ion.

Both complexes appeared as ion distributions: more precisely, the ESI(+) spectra showed signals centered at $m/z = 1777.9$ and 1931.0, attributable to $[\mathbf{1} + H]^+$ and $[\mathbf{2} + H]^+$, respectively (Figures 5 and 6). As shown in the same figures, other signals were observed. The peaks occurring at $m/z = 1593.8$ and 1746.0 can be explained taking into account the loss of one dpm^- group, thus being related to the presence of the ions $[\mathbf{1} - dpm]^+$ and $[\mathbf{2} - dpm]^+$, respectively. Other peaks, i.e., the signals at $m/z = 606.4$ and 422.2, observed in both **1** and **2**, were assigned to $[Fe(dpm)_3 + H]^+$ and $[Fe(dpm)_2]^+$, respectively.

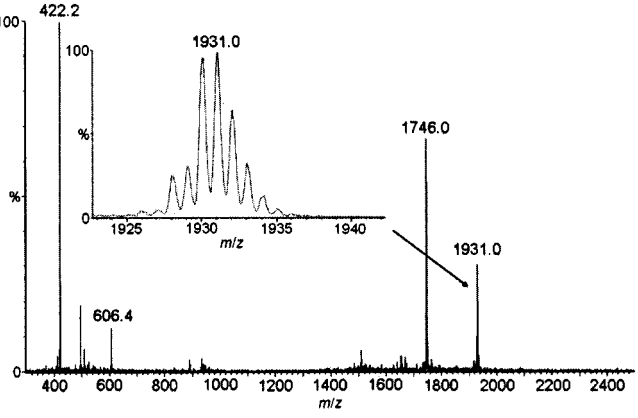

Figure 6. ESI(+)-MS full scan spectra of **2**. The inset shows a mass-scale-expanded segment of the ion signal at $m/z = 1931.0$ attributable to the $[\mathbf{2} + H]^+$ ion.

Magnetic Properties

The incorporation of two tripodal ligands in the structure of **3** is known to preserve the ground $S = 5$ spin state of the parent compound, at the same time producing a more than twofold increase of magnetic anisotropy (from $D = -0.20$ cm^{-1} in **3** to about -0.45 cm^{-1}).[10a,10b] The magnetic behavior of **1** and **2** was then compared in detail to support the proposed structural assignment. The molar magnetic susceptibility of **1** and **2**, reported in Figure 7 as a $\chi_m T$-versus-T plot, is characteristic of "ferric stars", where the dominant antiferromagnetic interaction between the central and peripheral high-spin iron(III) centers generates an $S = 5$ ground state.[10,11] The $\chi_m T$ product first decreases upon cooling down from room temperature, goes through a minimum at around 100 K, and then reaches a maximum at 10–15 K. Further cooling results again in a decrease of the magnetic moment. The value at the maximum (14.1–14.6 emu K mol^{-1}) is close to the Curie constant for an $S = 5$ state (15.0 emu K mol^{-1} for $g = 2.00$). The observation of a slightly lower magnetic moment, as well as the low-temperature decrease, is ascribed to saturation and/or anisotropy effects.

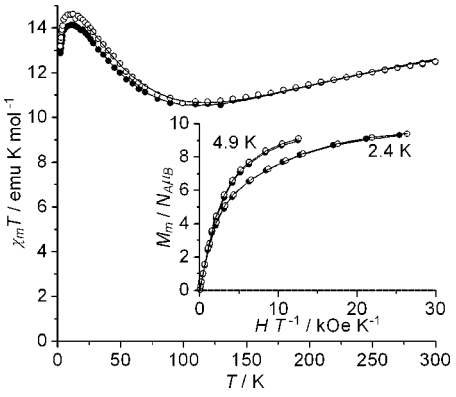

Figure 7. DC magnetic properties of **1** (open symbols) and **2** (solid symbols). The solid lines provide the best fit to the experimental data, as described in detail in the text.

Quantitative fitting of the data at $T > 20$ K using a Heisenberg spin-Hamiltonian with nearest-neighbor (J_1) and next-nearest-neighbor (J_2) coupling constants [Equation (1)] gives for **1**: $J_1 = 16.85(9)$ cm^{-1}, $J_2 = -0.07(9)$ cm^{-1}, and $g = 1.982(3)$; for **2**: $J_1 = 15.43(6)$ cm^{-1}, $J_2 = -0.54(5)$ cm^{-1}, and $g = 1.947(2)$.

$$\hat{\mathcal{H}}_0 = J_1(\hat{\mathbf{S}}_1\cdot\hat{\mathbf{S}}_2 + \hat{\mathbf{S}}_1\cdot\hat{\mathbf{S}}_3 + \hat{\mathbf{S}}_1\cdot\hat{\mathbf{S}}_4) + J_2(\hat{\mathbf{S}}_2\cdot\hat{\mathbf{S}}_3 + \hat{\mathbf{S}}_3\cdot\hat{\mathbf{S}}_4 + \hat{\mathbf{S}}_2\cdot\hat{\mathbf{S}}_4) + g\mu_B\hat{\mathbf{S}}\cdot\hat{\mathbf{H}} \quad (1)$$

As found in other Fe_4 complexes,[10a,10b] an accurate fit of magnetic data for **2** requires a small and ferromagnetic J_2 constant, though the real nature of next-nearest-neighbor interactions in this class of compounds remains to be fully ascertained. The isothermal molar magnetization measured at 4.9 and 2.4 K as a function of applied field (Figure 7, inset) approaches the appropriate value for an $S = 5$ state in high fields ($M_m/N_A\mu_B = 5g$). The fitting of experimental data with an axial zero-field splitting plus Zeeman Hamiltonian [Equation (2)] affords for **1**: $D = -0.450(5)$ cm^{-1} and $g = 1.983(3)$; for **2**: $D = -0.437(7)$ cm^{-1} and $g = 1.956(4)$.

$$\hat{\mathcal{H}}' = D[\hat{S}_z^2 - \tfrac{1}{3}S(S+1)] + g\mu_B\hat{\mathbf{S}}\cdot\hat{\mathbf{H}} \quad (2)$$

When imposing a positive D parameter, the fit is much worse, thus clearly indicating the presence of Ising-type magnetic anisotropy in both compounds.

These findings were confirmed by HF-EPR spectra recorded at 190 GHz as a function of temperature (Figure 8). For both species the typical behavior of an $S = 5$ state with easy-axis type anisotropy ($D < 0$) was observed. Indeed, at the highest temperature five parallel and five perpendicular transitions are detected for magnetic fields lower and higher than that corresponding to $g = 2.0$ ($H_0 = 66.7$ kOe), respectively, thus confirming the $S = 5$ ground state. On lowering the temperature, the lowest-field parallel transition and the highest-field perpendicular one gain intensity, as expected for $D < 0$.[18] The line-to-line separations, which in the high-field limit correspond to $2|D|/g_{\parallel}\mu_B$ for parallel transitions and to $|D|/g_{\perp}\mu_B$ for perpendicular ones, are consistent with a D value of about –0.43 cm^{-1}, which is characteristic of doubly substituted derivatives.[10a,10b] The spectra of **1** further evidence the presence of three isomers with slightly different zero-field splitting parameters. The relative intensity of the three signals is in the approximate ratio of 1:2:1, thus indicating that the three isomers are likely to arise from the disorder of the alkenyl chain. Indeed, given the two equally occupied positions (A and B) of the alkenyl chain observed in the X-ray structure, the three isomers should be AA (relative abundance = $0.5\times0.5 = 0.25$), AB = BA (relative abundance = $2\times0.5\times0.5 = 0.50$), and BB (relative abundance = $0.5\times0.5 = 0.25$).

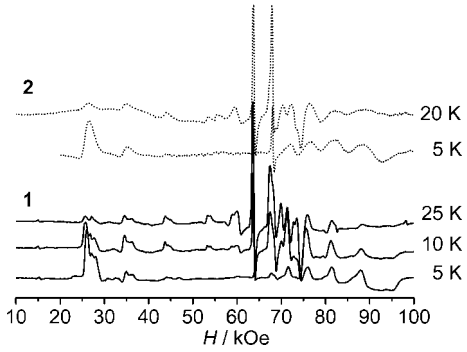

Figure 8. Temperature dependence of the HF-EPR spectra of **1** (continuous lines) and **2** (dotted lines) recorded at 190 GHz.

To obtain more detailed and precise information on the actual value of the zero-field splitting parameters, simulation of the spectra was undertaken. Given the monoclinic symmetry of derivative **1**, the following Hamiltonian was used for the simulation [Equation (3)].[19]

$$\hat{\mathcal{H}}_{EPR} = \mu_B\hat{\mathbf{S}}\cdot\mathbf{g}\cdot\hat{\mathbf{H}} + D\hat{\mathbf{S}}_z^2 + B_4^0\hat{\mathbf{O}}_4^0 + \frac{E}{2}\left(\hat{\mathbf{S}}_+^2 + \hat{\mathbf{S}}_-^2\right) \quad (3)$$

For both compounds g was fixed at 2.000 ± 0.005, as expected for high-spin iron(III)-containing species.[20] For derivative **1** a satisfactory simulation (Figure 9, left) at both 10 and 25 K was obtained assuming a relative abundance 1:2:1 for the three isomers, with the following parameters: $D_1 = -0.431$ cm^{-1}, $E_1 = 0.010$ cm^{-1}; $D_2 = -0.442$ cm^{-1}, $E_2 = 0.024$ cm^{-1}; $D_3 = -0.420$ cm^{-1}, $E_3 = 0.021$ cm^{-1}; with $B_4^0 = 1.0\times10^{-5}$ cm^{-1} for all isomers. The peculiar sharpness of the central lines of the spectrum has been accounted for by imposing different line widths for that group of resonances as well as by including the effect of a small distribution in the D and E values resulting from local strain-induced effects.

For compound **2**, the best simulations (Figure 9, right) were obtained with $D = -0.435$ cm^{-1}, $E = 0.018$ cm^{-1}, and $B_4^0 = 1.5\times10^{-5}$ cm^{-1}. The peculiar differences in line widths along the spectrum have been accounted for in the same way as for **1**. However, for this derivative strain effects are much more evident, especially for the E parameter, as shown by the progressive broadening of the perpendicular transitions at higher fields.

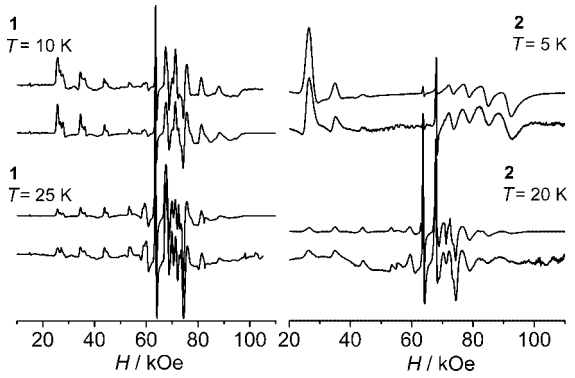

Figure 9. Best simulations (upper traces) of the experimental HF-EPR spectra recorded at 190 GHz (lower traces) at different temperatures for **1** (left) and **2** (right) obtained with the parameters reported in the text.

The zero-field splitting parameters obtained for **1** agree with the values expected on the basis of a recently proposed magnetostructural correlation between D, B_4^0, and the helical pitch γ.[10a] The presence of a small but non-negligible rhombic term ($E \neq 0$) confirms the deviation from ideal D_3 symmetry. The observation of slightly different D values for the three isomers of **1** further indicates that a small modification in the structure, even when not directly involving the core of the molecule, might affect, in a measurable way, the zero-field splitting parameters. Finally, on the basis of the above-mentioned magnetostructural correlation,[10a] the results obtained for **2** unambiguously prove the strict structural similarity between **2** and **1**.

The spin ground state and the easy-axis magnetic anisotropy evidenced above suggest that **1** and **2** may behave as SMMs at low temperature, as indeed observed for **3** and other simpler Fe_4 compounds.[10,11] We have therefore measured the AC susceptibility in zero static field and we have found, below 6 K, a nonzero imaginary component that goes through a frequency-dependent maximum on lowering the temperature. The behaviors of **1** and **2** are very similar, as can be seen in Figure 10. From the same data, the temperature dependence of the relaxation time τ has been extracted, assuming that when χ'' is maximum at a given frequency ν, the condition $\tau = (2\pi\nu)^{-1}$ is satisfied. A linear behavior of $\ln(\tau)$ as a function of $1/T$ is observed over the investigated frequency range, confirming a thermally activated mechanism for the relaxation (Figure 11). The best-fit parameters using the Arrhenius law $\tau = \tau_0 \exp(U_{eff}/k_B T)$ are for **1**: $\tau_0 = 3.4(1) \times 10^{-8}$ s, $U_{eff}/k_B = 15.9(2)$ K; for **2**: $\tau_0 = 4.3(1) \times 10^{-8}$ s, $U_{eff}/k_B = 15.1(2)$ K. The U_{eff} values are close to the anisotropy barriers predicted for integer spins by the formula $U = |D|S^2$, which neglects QT effects, as found in other doubly substituted Fe_4 derivatives.[10a,10b] The pre-exponential factors τ_0 are also quite similar to those observed with simpler triols,[10a] suggesting that the bulkier and more flexible long aliphatic chains of **1** and **2** do not affect the spin-phonon coupling in a significant way.

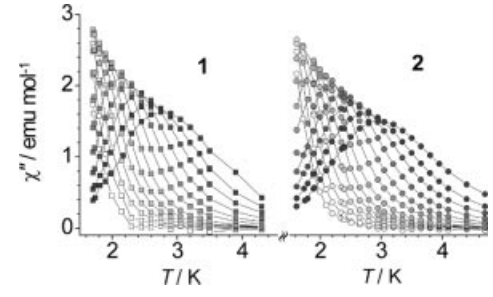

Figure 10. Imaginary component of the AC susceptibility measured for **1** (left) and **2** (right) in zero static field in the frequency range from 100 Hz (white) to 25 kHz (black).

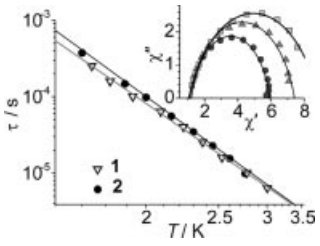

Figure 11. Temperature dependence of the relaxation time for **1** and **2**. The lines represent the best-fit curves using the Arrhenius law. The inset shows the Argand plot for **2** at 2.5 K (circles), 2.0 K (triangles), and 1.75 K (squares). The lines represent the best-fit curves using a modified Debye model. Susceptibilities are in emu mol^{-1}.

We have also investigated how the presence of different isomers, evidenced in **1**, or the sizeable strain effects in **2** influence the distribution of relaxation times. By plotting χ'' versus χ' at a given temperature, a semicircumference centered on the x axis should be observed in the absence of distribution, according to the Debye model.[21] The results are shown in the inset of Figure 11 for **2** and in Figure S3 of the Supporting Information for **1**. The presence of a distribution of relaxation times is accounted for by a parameter α[1b,21] which has been evaluated for **1** and **2** and is found to increase on lowering the temperature to reach 0.26 at 1.75 K for both compounds. The closest-to-the-origin intercept of the semicircle with the x axis represents the fraction of the magnetic susceptibility that relaxes much faster than the employed frequencies. Interestingly, both compounds show an almost temperature-independent fast relaxing component of the AC susceptibility of about 1 emu mol^{-1}. This value agrees well with the transverse component of the susceptibility of our randomly oriented powder samples evaluated by using the spin Hamiltonian parameters determined from HF-EPR experiments. The transverse component is not expected to experience any barrier when reversing its direction and thus is expected to relax much faster than the investigated frequency domain.

Conclusions

Single-molecule magnets functionalized with terminal alkenyl and thioacetyl groups have been prepared by site-specific substitution on the complex $[Fe_4(OMe)_6(dpm)_6]$ (**3**) using derivatives of 2-(hydroxymethyl)propane-1,3-diol as incoming ligands. The two tripods are located along the

idealized threefold molecular axis, leading to wire-like molecular geometries, which are particularly well suited for the construction of metal-molecule-metal junctions. The complexes are found to be stable in solution and afford intense molecular peaks in the ESI-MS spectra. The magnetic properties, as revealed by DC and AC magnetometry and HF-EPR spectroscopy, indicate that the compounds have an $S = 5$ ground spin state. The easy-axis anisotropy is enhanced as compared with **3** and the effective energy barrier reaches up to 15–16 K, leading to slow relaxation of the magnetization at low temperature. We are currently investigating the formation of monolayers of **1** and **2** on H-terminated Si(100) (by hydrosilylation) and Au(111), respectively. The estimated distance between the thioacetyl "alligator clips" in **2** is 2.8–2.9 nm, and the molecule is then expected to fit into state-of-the-art metal nanogaps prepared using break junctions or electromigration.[6]

Experimental Section

Synthesis: All chemicals were reagent-grade and used as received, unless otherwise noted. Diethyl ether, benzene, and toluene were distilled from sodium/benzophenone shortly before use. Benzene and toluene were stored over KOH pellets. Methanol was carefully dried by treatment with Mg/I_2 and distilled prior to use.[22] Dimethoxyethane (DME) was distilled from NaH. 2,2-Bis(hydroxymethyl)-10-undecen-1-ol (H_3L^1) was prepared by CaO-catalyzed Tollens reaction of 10-undecenal and formaldehyde in an EtOH/water mixture, according to a literature procedure.[13a] The precursor $[Fe_4(OMe)_6(dpm)_6]$ (**3**) and its deuterated variant, $[Fe_4(OMe)_6([D_{18}]dpm)_6]$ (**3D**), were prepared as described elsewhere.[10a]

11-(Acetylthio)-2,2-bis(hydroxymethyl)undecan-1-ol (H_3L^2): Thioacetic acid (0.660 g, 8.67 mmol) and 2,2′-azobis(2-methylpropionitrile) (0.713 g, 4.34 mmol) were added to a hot solution of H_3L^1 (1.00 g, 4.34 mmol) in dry benzene (10 mL). After stirring for 4 h at reflux temperature, the solution was cooled down and diethyl ether was added. The organic mixture was washed with saturated $NaHCO_3$ solution (3×) and brine. The solution was dried with Na_2SO_4 and filtered. After purification by column chromatography (eluent ethyl acetate/petroleum ether = 3:1), the product H_3L^2 was obtained as a white solid (0.745 g, 56%). ^{1}H NMR (300 MHz, $CDCl_3$, 25 °C): δ = 3.74 [s, 6 H, C(1)H_2], 2.86 [t, J = 2.0 Hz, 2 H, C(11)H_2], 2.47 (br. s, 3 H, OH), 2.32 (s, 3 H, CH_3), 1.62 [m, 2 H, C(10)H_2], 1.56 [m, 2 H, C(9)H_2], 1.40–1.10 (m, 12 H, Aliph) ppm. $C_{15}H_{30}O_4S_1$ (306.46): calcd. C 58.79, H 9.87, S 10.46; found C 58.58, H 9.96, S 10.32.

$[Fe_4(L^1)_2(dpm)_6]$ (1): Solid H_3L^1 (0.132 g, 0.573 mmol) and **3** (0.180 g, 0.119 mmol) were thoroughly mixed and heated to 70 °C under vacuum (0.1 Torr) for 15 min. The mixture was cooled down, powdered again, and reheated under the same conditions. After cooling, the solid was dissolved in dry toluene (12 mL) with gentle heating. Vapor diffusion of dry methanol (40 mL) into the filtered dark-orange solution afforded large dark-red blocks, which were washed with the external solvent mixture followed by pure methanol and then dried under vacuum (0.201 g, 95%). $C_{92}H_{160}Fe_4O_{18}$ (1777.60): calcd. C 62.16, H 9.07; found C 61.53, H 9.33. FTIR (KBr pellet): $\tilde{\nu}$ = 3080 (=C–H stretching), 1644 (C=C stretching), 994 (out-of-plane =C–H bending), 909 (in-plane =C–H bending) cm^{-1}.

$[Fe_4(L^2)_2(dpm)_6]$ (2): H_3L^2 (0.0658 g, 0.215 mmol) and **3** (0.120 g, 0.0795 mmol) were dissolved in dry DME/Et_2O (1:1, v/v) (20 mL) with prolonged stirring. By slow concentration of the clear yellow-orange solution, a crystalline red-orange solid was obtained, which was washed with dry DME/MeOH (1:5, v/v) and dried under vacuum (0.1 Torr, 1 h) (0.138 g, 90%). $C_{96}H_{168}Fe_4O_{20}S_2$ (1929.89): calcd. C 59.75, H 8.77, S 3.32; found C 59.51, H 9.25, S 3.53. FTIR (KBr pellet): $\tilde{\nu}$ = 1699 (C=O stretching) cm^{-1}.

X-ray Crystallography: A single-crystal X-ray study was carried out on **1** with a four-circle Bruker X8APEX diffractometer equipped with a Kryo-Flex cryostat and controlled by Bruker-Nonius X8APEX software. Crystal structure data: $C_{92}H_{160}Fe_4O_{18}$, M_r = 1777.60, crystal dimensions $0.42 \times 0.30 \times 0.24$ mm, monoclinic, space group $C2/c$ (no. 15), a = 23.9416(3), b = 15.6441(2), c = 27.1433(4) Å, β = 95.8450(10)°, V = 10113.5(2) Å^3, Z = 4, $\rho_{calcd.}$ = 1.167 g cm^{-3}, $2\theta_{max}$ = 52.02, Mo-K_α radiation, λ = 0.71073 Å, T = 120(2) K, μ = 0.621 mm^{-1}, collected/independent reflections 73989/9888 [R(int) = 0.0260]. The structure was solved by direct methods using the SIR92[23a] program. Full-matrix least-squares refinement on F_o^2 was performed using the SHELXL-97 program[23b] implemented in the WINGX suite[23c] on 9888 data points with 596 parameters and 43 restraints. All non-hydrogen atoms were refined anisotropically, and hydrogen atoms were added in idealized positions and assigned isotropic displacement parameters 50% and 20% larger than the U_{eq} of the attached carbon atoms for aliphatic and methine hydrogen atoms, respectively. The alkyl chain of the tripodal ligand was found to be disordered over two equally populated positions. Final R indices [$I > 2\sigma(I)$]: R_1 = 0.0425, wR_2 = 0.1113; R indices (on all data): R_1 = 0.0593, wR_2 = 0.1298. Goodness-of-fit on F^2 = 1.031. Largest difference peak/hole 0.989/–0.667 e Å^{-3}. CCDC-646831 contains the supplementary crystallographic data for this paper. These data can be obtained free of charge from The Cambridge Crystallographic Data Centre via www.ccdc.cam.ac.uk/data_request/cif.

Physical Techniques: NMR spectra of the complexes were recorded at 302 K with a Bruker FT-DPX200 NMR spectrometer. Samples for ^{1}H NMR spectroscopy were solutions of **1** and **2** in $CDCl_3$ (concentration about 13.5 mg/mL). Samples for ^{2}H NMR spectroscopy were solutions of **3D** in dry Et_2O (about 2.6 mg/mL), to which solid H_3L^1 or H_3L^2 (2.7 equiv.) was added. Chemical shifts were referenced to [D_6]acetone as external standard (δ =2.16 ppm). IR spectra were recorded with an FTIR Perkin–Elmer 1600 spectrometer. Samples were ground thoroughly with KBr at approximately 1% by weight and pressed into a pellet with a thickness of about 1 mm. UV/Vis spectra in the range 200–900 nm were recorded in toluene solution with a UV/Vis Perkin–Elmer λ650 spectrometer using quartz cuvettes with a 1-mm optical path. Electrospray mass spectra were acquired with a Micromass® Q-TOF micro™ mass spectrometer (Waters, UK) equipped with a Z-spray electrospray interface. Masslynx v. 3.5 software (Micromass) was used for data acquisition and processing. ESI-MS analyses were performed by operating the mass spectrometer in positive-ion (PI) mode acquiring mass spectra over the scan range m/z = 300–2500, with a scan time of 1.2 s and an interscan delay of 0.1 s. The nebulizing gas (nitrogen, 99.999% purity) and the desolvation gas (nitrogen, 99.999% purity) were delivered at a flow rate of 150 and 600 l h^{-1}, respectively. The operating parameters of the interface were as follows: source temperature 90 °C, desolvation temperature 150 °C, cone voltage 30 V, ES (+) voltage 3.5 and 4.0 kV for the analysis of **1** and **2**, respectively. Q-TOF external calibration was performed using 0.1% (v/v) aqueous phosphoric acid solution. DC magnetic data were recorded using a Cryogenic S600 SQUID magnetometer. Susceptibility versus T data from 2.2 to 300 K were collected on 22.75- and 31.80-mg microcrystalline samples of **1** and **2** with applied fields of 10 kOe (for $T > 30$ K) and 1 kOe (for $T <$

30 K) in order to reduce saturation effects. Isothermal magnetization versus H curves were registered up to 60 kOe at about 2.4 and 4.9 K. Raw data were reduced with molecular weights equal to 1777.60 (**1**) and 1929.89 (**2**) and using diamagnetic corrections estimated from Pascal's constants -1061.74×10^{-6} and -1146.72×10^{-6} emu mol^{-1} for **1** and **2**, respectively. The AC susceptibility of microcrystalline samples of **1** and **2** has been measured in the frequency range 100–25000 Hz with a home-made susceptometer[24] based on an Oxford Instruments MAGLAB2000 platform. High-frequency EPR (HF-EPR) spectra were recorded at the Grenoble High Magnetic Field Laboratory with a home-built spectrometer working in single-pass mode using a Gunn diode working at 95 GHz equipped with a frequency doubler as source excitation. Samples were pressed in pellets to avoid orientation effects.

Spin Hamiltonian Calculations: The NAG Fortran Library Routine E04FCF[25a] was used for fitting magnetic susceptibility and magnetization data with the aid of the ZHEEV routine (LAPACK Linear Algebra Package) for matrix diagonalization.[25b] Calculations were carried out with a Digital Alpha3000/800S computer.

Supporting Information (see footnote on the first page of this article): UV/Vis, IR, and fully labeled ESI-MS spectra for **1** and **2**, and Argand plot for **1**.

Acknowledgments

This work was supported by the European Union through RTN "QUEMOLNA" (FP6-CT-2003-504880), NE "MAGMANET" (FP6-NMP3-CT-2005-515767), and NanoSci-ERA Project "SMMTRANS". Funding by Italian Ministero dell'Università e della Ricerca (MIUR) through FISR, FIRB, and PRIN projects is also acknowledged. We thank Rossella Gallesi (Department of Pharmaceutical Sciences, Università degli Studi di Modena e Reggio Emilia) for elemental analysis.

[1] a) R. Sessoli, D. Gatteschi, A. Caneschi, M. A. Novak, *Nature* **1993**, *365*, 141–143; b) D. Gatteschi, R. Sessoli, J. Villain, *Molecular Nanomagnets*, Oxford University Press, Oxford, **2006**.

[2] a) L. Thomas, F. Lionti, R. Ballou, D. Gatteschi, R. Sessoli, B. Barbara, *Nature* **1996**, *383*, 145–147; b) J. Friedman, M. P. Sarachick, J. Tejada, R. Ziolo, *Phys. Rev. Lett.* **1996**, *76*, 3830–3833; c) D. Gatteschi, R. Sessoli, *Angew. Chem. Int. Ed.* **2003**, *42*, 268–297.

[3] C. J. Milios, A. Vinslava, W. Wernsdorfer, S. Moggach, S. Parsons, S. P. Perlepes, G. Christou, E. K. Brechin, *J. Am. Chem. Soc.* **2007**, *129*, 2754–2755.

[4] A. Cornia, A. Fabretti Costantino, L. Zobbi, A. Caneschi, D. Gatteschi, M. Mannini, R. Sessoli, *Struct. Bond.* **2006**, *122*, 133–161.

[5] a) R. V. Martínez, F. García, R. García, E. Coronado, A. Forment-Aliaga, F. M. Romero, S. Tatay, *Adv. Mater.* **2007**, *19*, 291–295; b) R. W. Saalfrank, A. Scheurer, I. Bernt, F. W. Heinemann, A. V. Postnikov, V. Schünemann, A. X. Trautwein, M. S. Alam, H. Rupp, P. Müller, *Dalton Trans.* **2006**, 2865–2874; c) L. Zobbi, M. Mannini, M. Pacchioni, G. Chastanet, D. Bonacchi, C. Zanardi, R. Biagi, U. Del Pennino, D. Gatteschi, A. Cornia, R. Sessoli, *Chem. Commun.* **2005**, 1640–1642.

[6] a) H. B. Heersche, Z. de Groot, J. A. Folk, H. S. J. van der Zant, C. Romeike, M. R. Wegewijs, L. Zobbi, D. Barreca, E. Tondello, A. Cornia, *Phys. Rev. Lett.* **2006**, *96*, 206801/1–4; b) M.-H. Jo, J. Grose, K. Baheti, M. M. Deshmukh, J. J. Sokol, E. M. Rumberger, D. N. Hendrickson, J. R. Long, H. Park, D. C. Ralph, *Nano Lett.* **2006**, *6*, 2014–2020; c) J. J. Henderson, C. M. Ramsey, E. del Barco, A. Mishra, G. Christou, *J. Appl. Phys.* **2007**, *101*, O9E102/1-3.

[7] M. Pacchioni, A. Cornia, A. C. Fabretti, L. Zobbi, D. Bonacchi, A. Caneschi, G. Chastanet, D. Gatteschi, R. Sessoli, *Chem. Commun.* **2004**, 2604–2605.

[8] a) T. Strother, W. Cai, X. Zhao, R. J. Hamers, L. M. Smith, *J. Am. Chem. Soc.* **2000**, *122*, 1205–1209; b) Y. Kang, D.-J. Won, S. R. Kim, K. Seo, H.-S. Choi, G. Lee, Z. Noh, T. S. Lee, C. Lee, *Mater. Sci. Eng. C* **2004**, *24*, 43–46.

[9] E. K. Brechin, *Chem. Commun.* **2005**, 5141–5153.

[10] a) S. Accorsi, A. L. Barra, A. Caneschi, G. Chastanet, A. Cornia, A. C. Fabretti, D. Gatteschi, C. Mortalò, E. Olivieri, F. Parenti, P. Rosa, R. Sessoli, L. Sorace, W. Wernsdorfer, L. Zobbi, *J. Am. Chem. Soc.* **2006**, *128*, 4742–4755; b) A. Cornia, A. C. Fabretti, P. Garrisi, C. Mortalò, D. Bonacchi, D. Gatteschi, R. Sessoli, L. Sorace, W. Wernsdorfer, A.-L. Barra, *Angew. Chem. Int. Ed.* **2004**, *43*, 1136–1139; c) M. Moragues-Canovas, E. Riviere, L. Ricard, C. Paulsen, W. Wernsdorfer, G. Rajaraman, E. K. Brechin, T. Mallah, *Adv. Mater.* **2004**, *16*, 1101–1105.

[11] A. L. Barra, A. Caneschi, A. Cornia, F. Fabrizi de Biani, D. Gatteschi, C. Sangregorio, R. Sessoli, L. Sorace, *J. Am. Chem. Soc.* **1999**, *121*, 5302–5310.

[12] R. W. Saalfrank, I. Bernt, M. M. Chowdhry, F. Hampel, G. B. M. Vaughan, *Chem. Eur. J.* **2001**, *7*, 2765–2769.

[13] a) A. Muth, A. Asam, G. Huttner, A. Barth, L. Zsolnai, *Chem. Ber.* **1994**, *127*, 305–311; b) V. Gagnard, A. Leydet, A. Morère, J.-L. Montero, I. Lefèbvre, G. Gosselin, C. Pannecouque, E. De Clercq, *Bioorg. Med. Chem.* **2004**, *12*, 1393–1402.

[14] D. Gatteschi, L. Sorace, *J. Solid State Chem.* **2001**, *159*, 253–261.

[15] R. L. Lintvedt, L. K. Kernitsky, *Inorg. Chem.* **1970**, *9*, 491–494.

[16] a) J. B. Fenn, M. Mann, C. K. Meng, S. F. Wong, C. M. Whitehouse, *Science* **1989**, *246*, 64–71; b) I. Jardine, *Nature* **1990**, *345*, 747–748.

[17] a) V. Katta, S. K. Chowdhury, B. T. Chait, *J. Am. Chem. Soc.* **1990**, *112*, 5348–5349; b) T. G. Spence, T. D. Burns, G. B. Guckenberger, V. A. Posey, *J. Phys. Chem. A* **1997**, *101*, 1081–1092; c) E. Coronado, M. Feliz, A. Forment-Aliaga, C. J. Gomez-Garcia, R. Llusar, F. M. Romero, *Inorg. Chem.* **2001**, *40*, 6084–6085; d) H. Zhao, C. P. Berlinguette, J. Bacsa, A. V. Prosvirin, J. K. Bera, S. E. Tichy, E. J. Schelter, K. R. Dunbar, *Inorg. Chem.* **2004**, *43*, 1359–1369; e) P. Pelagatti, A. Bacchi, F. Calbiani, M. Carcelli, L. Elviri, C. Pelizzi, D. Rogolino, *J. Organomet. Chem.* **2005**, *690*, 4602–4610.

[18] A. L. Barra, L.-C. Brunel, D. Gatteschi, L. Pardi, R. Sessoli, *Acc. Chem. Res.* **1998**, *31*, 460–466.

[19] C. J. H. Jacobsen, E. Pedersen, J. Villadsen, H. Weihe, *Inorg. Chem.* **1993**, *32*, 1216–1221.

[20] J. R. Pilbrow, *Transition Ion Electron Paramagnetic Resonance*, Clarendon Press, Oxford, **1990**.

[21] a) K. S. Cole, R. H. Cole, *J. Chem. Phys.* **1941**, *9*, 341–351; b) C. Dekker, A. F. M. Arts, H. W. Wijn, A. J. van Duyneveldt, J. A. Mydosh, *Phys. Rev. B* **1989**, *40*, 11243–11251.

[22] A. I. Vogel, *Practical Organic Chemistry*, Longman, London, **1959**.

[23] a) A. Altomare, G. Cascarano, C. Giacovazzo, A. Guagliardi, *J. Appl. Crystallogr.* **1993**, *26*, 343–350; b) G. M. Sheldrick, *SHELX97, Programs for Crystal Structure Analysis (Release 97-2)*, University of Göttingen, Göttingen, **1997**; c) L. J. Farrugia, *J. Appl. Crystallogr.* **1999**, *32*, 837–838.

[24] S. Midollini, A. Orlandini, P. Rosa, L. Sorace, *Inorg. Chem.* **2005**, *44*, 2060–2066.

[25] a) *E04FCF, NAG Fortran Library Routine (Mark 17)*, NAG Ltd, Oxford, **1996**; b) *ZHEEV, LAPACK driver routine (Version 2.0)*, University of Tennessee, University of California Berkeley, NAG Ltd., Courant Institute, Argonne National Lab, Rice University, **1994**.

Received: April 5, 2007
Published Online: July 17, 2007

